



# Tunable magnetoresistance in Li<sub>2</sub>BaSi

Vineet Kumar Sharma, V. Kanchana\*

Department of Physics, Indian Institute of Technology Hyderabad, Kandi - 502285, Sangareddy, Telangana, India

## ARTICLE INFO

### Article history:

Received 23 May 2022

Received in revised form 30 September 2022

Accepted 7 November 2022

Available online 10 November 2022

Communicated by L.M. Woods

### Keywords:

Electronic band structure

Large magnetoresistance

Tunable magnetotransport

## ABSTRACT

We present the magnetotransport behavior of Li<sub>2</sub>BaSi using Boltzmann transport theory within relaxation time approximation. The semimetallic nature and anisotropic band dispersion suggest a possible large magnetoresistance. The electrical resistivities and magnetoresistance display non-saturating behavior for low magnetic field values and get saturated at higher fields due to charge-carrier uncompensation and are almost similar with and without spin-orbit coupling. Shifting the Fermi level by 0.10 eV results in tunable magnetotransport features with improved transverse MR values up to 200% for 12 T at 10 K with non-saturating behavior. Our calculations predict that this investigated compound can be deemed a better MR material for its transverse effects.

© 2022 Elsevier B.V. All rights reserved.

## 1. Introduction

The change in electrical resistance that occurs when a material is exposed to an external magnetic field is known as magnetoresistance (MR).  $MR = [\rho(B) - \rho(0)]/\rho(0)$ , where  $\rho(0)$  and  $\rho(B)$  are, respectively, electrical resistivities at zero and non-zero values of applied magnetic field (B). The strength of the magnetic field and the angle between the magnetic field and the direction of current flow are both important factors in MR effects. There are two broad classes of MR, one is positive, and the other is negative MR. Positive MR occurs in metals, semiconductors, and semimetals, typically called Ordinary magnetoresistance (OMR), whereas the magnetic materials have negative MR. MR effects are relatively weak in most of the non-magnetic compounds, displaying quadratic field dependence in low fields. Manganese-based perovskite oxides composed of magnetic and non-magnetic layers have shown other MR effects such as giant magnetoresistance (GMR) [1,2] and colossal magnetoresistance (CMR) [3,4]. These systems show MR effects higher by several orders in magnitude compared to the values reported in non-magnetic cases. The high MR values are being utilized in terms of data storage in magnetic devices [5–7], which has gained the enormous attention towards the applied research in the magnetotransport phenomenon. The recent studies on different materials report the topological electronic phase and distinct features of MR with applied magnetic field in a low-temperature regime. These effects are different from the well-known MR ef-

fects like a giant MR with values of the order of 10<sup>6</sup> % at 0.4 K and 32 T field [8]) and colossal MR with a range of 10<sup>2</sup> to 10<sup>5</sup> % in oxide perovskites [9]. A very few such cases are being discussed here. The linear behavior of MR with the magnetic field was observed in Dirac semimetals like graphene and Cd<sub>3</sub>As<sub>2</sub> [10–14] and TaAs class of Weyl semimetals [15]. There are few other topological non-magnetic materials [16–22] that have shown quadratic field-dependent MR values. Different mechanisms were proposed to understand the reason behind the extremely large values of MR in non-magnetic materials. Topological protection could be a key player, but the classical two-band model can also be considered for quadratic field dependence of MR in carrier compensated semimetals similar to WTe<sub>2</sub> [17]. The magnetic field dependent electrical resistivities for a two-band model [23] can be written in terms of carriers density/concentration and their mobilities as:

$$\rho_{xx} = \frac{1}{e} \frac{(n_e \mu_e + n_h \mu_h) + (n_e \mu_e \mu_h^2 + n_h \mu_h \mu_e^2) B^2}{(n_e \mu_e + n_h \mu_h)^2 + (n_e - n_h)^2 \mu_e^2 \mu_h^2 B^2} \quad (1)$$

$$\rho_{xy} = \frac{1}{e} \frac{(n_h \mu_h^2 - n_e \mu_e^2) B + \mu_e^2 \mu_h^2 (n_h - n_e) B^3}{(n_e \mu_e + n_h \mu_h)^2 + (n_e - n_h)^2 \mu_e^2 \mu_h^2 B^2} \quad (2)$$

For a semimetal, where  $n_h = n_e$  and  $\mu_h = \mu_e$ , MR turns out to be non-saturating as it varies quadratically with magnetic field (B). MR effects can be observed in topologically trivial cases too [24–35], where Fermi surface topology is used as a prominent mechanism for understanding the large values of MR. The topology in Fermi surfaces is connected to the motion of electrons, which divides the metals into three distinct classes. The first class of metals contains the closed Fermi surfaces, and the

\* Corresponding author.

E-mail address: [kanchana@iith.ac.in](mailto:kanchana@iith.ac.in) (V. Kanchana).

electrons are constrained to their orbits. These metals display the saturation of MR for large magnetic fields. Some metals, such as Bi, Sb, W, Mo, etc., show perfect charge carrier compensation with equal holes and electrons, leading to non-saturating MR. Some other metals have a combination of both open and closed Fermi surfaces, exhibiting large MR along the axes with open Fermi surfaces. In contrast, it saturates in other directions, where the Fermi surfaces are closed. Given the relevance of the Fermi surface in magnetotransport, a plethora of models with basic geometrical forms have been developed. The model for magneto-conductivity in Bismuth devised by many groups is the most successful example [36,37]. Experimentalists have reported magnetotransport in a variety of topological materials, including Dirac, Weyl, and nodal line semimetals [10–15,38,39]. It is observed that out of three different cases discussed on Fermi surface topology, the charge carrier compensation approach, including the two-band model, has been used for elaborating the magnetotransport phenomena. The discussion as mentioned above together with previous studies on nodal line semimetals [40,41] motivate us to choose  $\text{Li}_2\text{BaSi}$  class of semimetals for their magnetotransport phenomena. V.K. Sharma et al. extensively studied the electronic structure properties and phonon dispersion of  $\text{Li}_2\text{BaSi}$ . The detailed analysis of phonon dispersion displayed interesting topological phononic states, immune to backscattering due to the non-zero Berry phase, and might be suitable for phonon waveguide applications. Additionally, the electronic structure properties revealed it to be an inner nodal chain semimetal in the absence of spin-orbit coupling (SOC), and it transits to a trivial topological insulator under SOC [40]. The coexistence of both electron and phonon topology is rarely discussed in the same material, enabling  $\text{Li}_2\text{BaSi}$  more plausible nodal line material than the others. The observed transport properties of  $\text{Li}_2\text{BaSi}$  motivated us to opt this for our current work. We use the Boltzmann transport theory within the relaxation time approximation to describe the temperature and magnetic field-dependent magnetotransport characteristics of  $\text{Li}_2\text{BaSi}$  and notice the tunability in magnetoresistance with carrier doping in this paper. The layout of this paper is as follows: section 2 explains the computational methods used in our calculations, followed by section 3 describing the electronic properties. Magnetic field and temperature dependent magnetotransport calculations are given in section 4 at ambient. The variation in MR values via Fermi energy shifting for possible future doping effects is written in section 5, and section 6 concludes the work.

## 2. Methodology

The structural optimization is performed using VASP [42,43] for different exchange-correlation functionals, GGA-PBE [44] and LDA [45]. GGA parameters ( $a = 6.69 \text{ \AA}$ ,  $b = 4.66 \text{ \AA}$  and  $c = 6.38 \text{ \AA}$ ) are consistent with experiments ( $a = 6.74 \text{ \AA}$ ,  $b = 4.68 \text{ \AA}$  and  $c = 6.26 \text{ \AA}$ ) [46]. A  $9 \times 9 \times 9$  K-mesh [47] is used with the convergence conditions for energy and tolerance factor to be  $10^{-8} \text{ eV}$  and  $10^{-2} \text{ eV/\AA}$ , respectively. The energy cut-off is set to 900 eV. Tetrahedron method [48] is used for Brillouin zone integration. VASP is used to calculate electronic structural parameters like band structure and Fermi surface. The magnetic field-dependent conductivity tensor is computed using semi-classical Boltzmann transport theory within the relaxation time approximation [49–52] utilizing the combination of VASP2 WANNIER90 and Wannier90 programmes [53–56].

To investigate the influence of both temperature and magnetic field on these computations, we have employed magnetic fields ranging from 0–12 T and temperatures ranging from 50 K to 300 K.  $\rho = \sigma^{-1}$  is used to compute the resistivity. The crystal structure of  $\text{Li}_2\text{BaSi}$ , which has a non-centrosymmetric orthorhombic symmetry and the space group  $\text{Pmmn}(59)$ , is shown in Fig. 1(a). Fig. 1(b) depicts the irreducible Brillouin zone with high symmetry points.

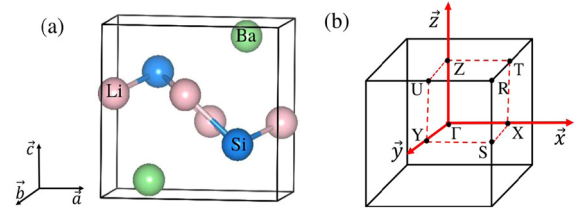


**Fig. 1.** (a) Crystal Structure and (b) the irreducible Brillouin zone. The light pink, blue, and green spheres depict Li, Si, and Ba atoms, respectively. (For interpretation of the colors in the figure(s), the reader is referred to the web version of this article.)

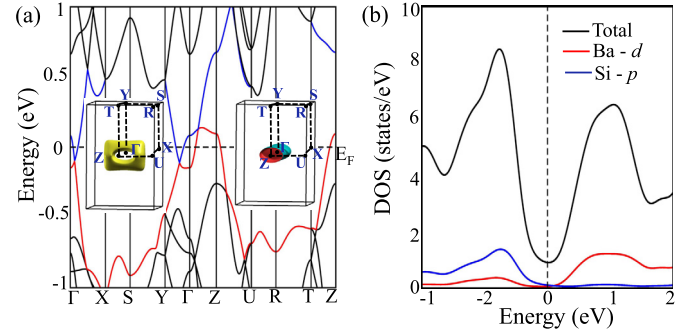


**Fig. 2.** (a) The electronic band structure is plotted along high symmetry points, as mentioned in IBZ Fig. 1(b). The Fermi surfaces for both bands are shown as insets. The high-symmetry points are depicted on the Fermi surface to commensurate the band dispersion along all the crystallographic axes. (b) The density of states along with the partial contribution.

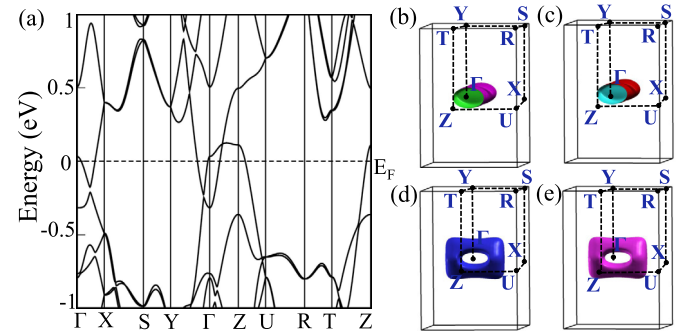


**Fig. 3.** The electronic structure properties with spin-orbit coupling (a) The electronic band structure plotted along high symmetry points, as mentioned in IBZ Fig. 1(b). The Fermi surfaces for both bands are shown in Figures (b-e).

## 3. Electronic structure properties

We present the electronic structure properties such as band structure and density of states of  $\text{Li}_2\text{BaSi}$  in Fig. 2. We can see the fascinating Dirac-like band crossings along the band paths  $\Gamma - X$ ,  $\Gamma - Y$ , and  $\Gamma - Z$ . The hole and electron-type bands near the Fermi level confirm the semimetallic state. The parity analysis suggests that these bands have opposite mirror eigenvalues,  $B_{3u}$  (electron band) and  $A_{1g}$  (hole band), and certifies the band inversion at  $\Gamma$  point. We have plotted the total and projected density of states [Fig. 2(b)]. We can see a crossover between the electron and hole bands which are mainly contributed by Ba -  $d$  and Si -  $p$  states. The inclusion of spin-orbit coupling (SOC) becomes important whenever such features are present in the electronic band structure of a material. Thus, we have included the same, which are shown in Fig. 3. The SOC lifts the degeneracy and opens the gap between crossing points. The topological features of these band crossings are documented in the previous study [40], reporting the formation of a nodal chain state consisting of nodal loops in  $k_z = 0$  and

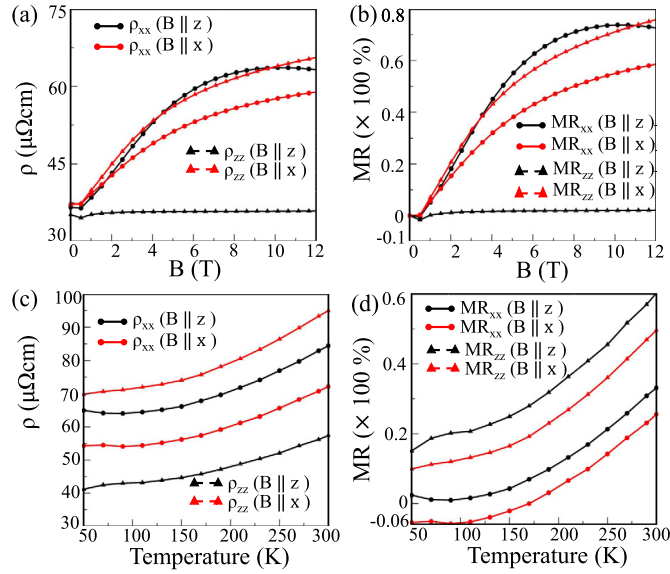


**Fig. 4.** (a) The resistivity as a function of applied magnetic field at 10 K. (b) The magnetoresistance as a function of magnetic field for 10 K, (c) Temperature-dependent resistivity and magnetoresistance for a magnetic field value of 10 T are given in (c) and (d), respectively.

$k_y = 0$  planes when SOC is ignored. There was a non-trivial nodal chain state transforming to a trivial insulating state with SOC.

Next, we discuss the Fermi surface, whose shapes are crucial in superconductors. For example, the sheet-like Fermi surface leads to Fermi-surface nesting, which further results in charge and spin density waves [57]. The recent studies on Fermi surface topology signified its importance in magneto-transport properties like magnetoresistance [58]. The Fermi surface plots for both bands are shown in insets of Fig. 2(a). The electron-type Fermi surface is shown on the left side as the band crosses the Fermi level from the conduction band to the valence band. The hole-type Fermi surface is depicted on the right side as the corresponding band crosses the Fermi level from the valence band to the conduction band. The shape of the electron-like Fermi surface resembles the cuboid with an elliptical hole centered around  $\Gamma$  point. The hole-like Fermi surface is a combination of open and closed ends due to the band dispersion of the corresponding band in  $k_z = 0.5$  plane. We have plotted the Fermi surfaces under SOC which are similar to what we discussed in the case of without SOC, and the number of Fermi surfaces is doubled due to doubly-degenerate bands [Fig. 3(b-e)]. The close observation of band dispersion indicates its anisotropic nature, resulting in anisotropic Fermi surfaces, which may host large magnetoresistance here.

#### 4. Magnetoresistance calculations

The above-discussed interesting electronic properties in  $\text{Li}_2\text{BaSi}$  motivate us to explore the effect of the magnetic field on its electrical resistivity using Boltzmann transport theory within relaxation time approximation. In the present case, two bands are crossing the Fermi level; one corresponds to hole nature and the other to electron nature [Fig. 2]. We would like to project their combined effect in terms of total resistivity and MR [the sum of both the hole and electron contributions]. We have computed the electrical resistivity both along 'x' and 'z' directions to observe transverse and longitudinal effects of the magnetic field applied. Total resistivity as a function of magnetic field is shown in Fig. 4(a). Depending on the mutual direction of the current and magnetic field, both  $\rho_{xx}$  and  $\rho_{zz}$  can be termed transverse and longitudinal

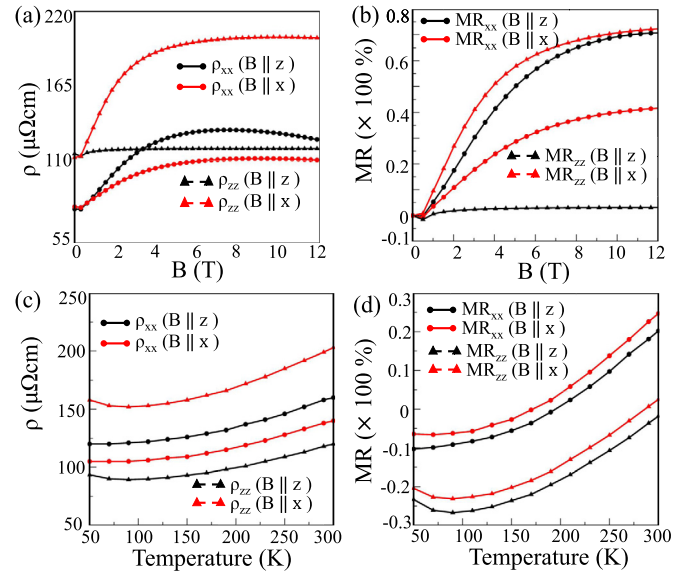


**Fig. 5.** Magnetotransport properties with spin-orbit coupling, (a) The resistivity as a function of applied magnetic field at 10 K. (b) The magnetoresistance as a function of magnetic field for 10 K, (c) Temperature-dependent resistivity and magnetoresistance for a magnetic field value of 10 T are given in (c) and (d), respectively.

resistivity. ( $B \perp I \rightarrow$  transverse resistivity and for  $B \parallel I \rightarrow$  longitudinal resistivity.)

One can see that the resistivity increases and reaches saturation after the magnetic field value of 10 T. The low-field resistivities are non-saturating, and we observe that the transverse resistivities are higher than the longitudinal ones. This trend in the resistivity curves is similar to ordinary magnetoresistance observed in metals or semimetals. The magnetic field-dependent MR corresponding to these resistivities is given in Fig. 4(b). Transverse MR values are higher than the longitudinal MR values with saturating behavior for high fields, as seen in the resistivity plots. The magnetic field orientation along 'z' direction has given better results with MR values of nearly 75% at 12 T for a temperature around 10 K. We have calculated both the electrical resistivities and MR for temperatures ranging from 50 K - 300 K at a fixed value of magnetic field 10 T [Fig. 4(c, d)] to capture the temperature effects. We have taken this magnetic field value to project the non-saturating region here. The resistivity and MR increase with the temperature, independent of magnetic field orientation, and show the non-saturating behavior with temperature. Both the longitudinal and transverse MR values are appreciable with 60% and 50% when B is along 'z' and 'x' directions, respectively at 300 K. These estimated values of MR are in line with the values reported for other well-known nodal line semimetals [59,60]. The noticed behavior of MR can be connected to Fermi surface topology as it entirely depends upon the velocity and cyclotron mass of electrons moving on these Fermi surfaces. We can see that the Fermi surface is anisotropic for both bands crossing the Fermi level.

The observed SOC effects in the electronic structure properties intend us to include the same in magnetotransport properties [Fig. 5]. The plots show that the resistivity values are higher with SOC than those without SOC, and it is non-saturating in a low-field regime and gets saturated for higher fields. The calculated MR values are almost similar to what we observed without SOC, which can be understood very well from the similar Fermi surfaces under SOC. The carrier-dependent electrical resistivities analysis suggests that the electrons are key carriers for magnetotransport behavior in  $\text{Li}_2\text{BaSi}$ . It ensures the absence of charge carrier compensation here which results in saturated MR at high fields.

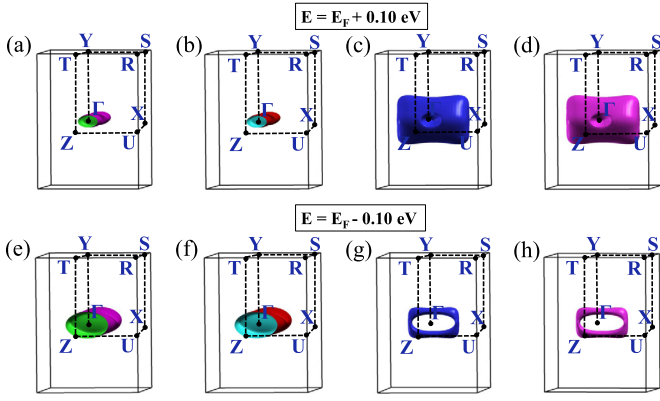


**Fig. 6.** The calculated Fermi surfaces at different Fermi energy values with spin-orbit coupling. (a-d) At  $E = E_F + 0.10$  eV and (e-h) at  $E = E_F - 0.10$  eV.

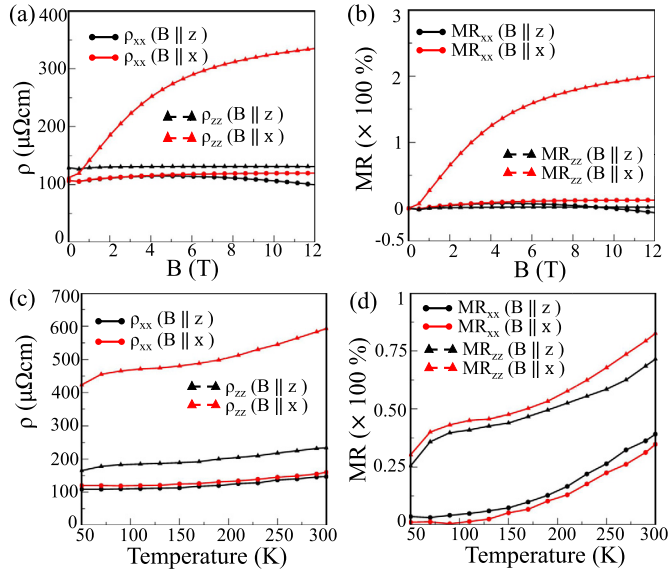


**Fig. 7.** (a) The resistivity and (b) the magnetoresistance as a function of magnetic field at a fixed temperature of 10 K, for  $E = E_F + 0.10$  eV. Temperature dependent resistivity, and magnetoresistance for a magnetic field value of 10 T are given in (c) and (d), respectively for  $E = E_F + 0.10$  eV.

## 5. Tunability in magnetoresistance

It would be interesting to see how the MR values would vary upon changing the chemical potential around the Fermi level. In addition, it may hint us about a favorable choice of doping to tune the magnetotransport properties. The Fermi surfaces at these Fermi energies are shown in Fig. 6. There are four Fermi surfaces in both case ( $E = E_F + 0.10$  eV &  $E = E_F - 0.10$  eV) due to spin-orbit coupling effects.

The magnetotransport properties at  $E = E_F + 0.10$  eV are given in Fig. 7.  $\rho_{zz}$  is appreciably high as well as non-saturating than the values calculated at the ambient case [Fig. 7(a)].  $\rho_{xx}$  shows non-saturating nature. Fig. 7(b) shows the magnetoresistance corresponding to these resistivities at 10 K. We can see that transverse MR values ( $MR_{zz}$ ) reach up to 200% when the magnetic field is along 'x' direction. This change can be connected to the Fermi surface topology. One can see the closed Fermi surface in this case [Fig. 6(c & d)], which is responsible for the improvement in  $MR_{zz}$  values when  $B \parallel x$ . This is due to changes in both the density of states and Fermi velocity at this Dirac-like crossing. Temperature-dependent resistivity is shown in Fig. 7(c), which is non-saturating and higher than the ambient values, and its effects can be seen on

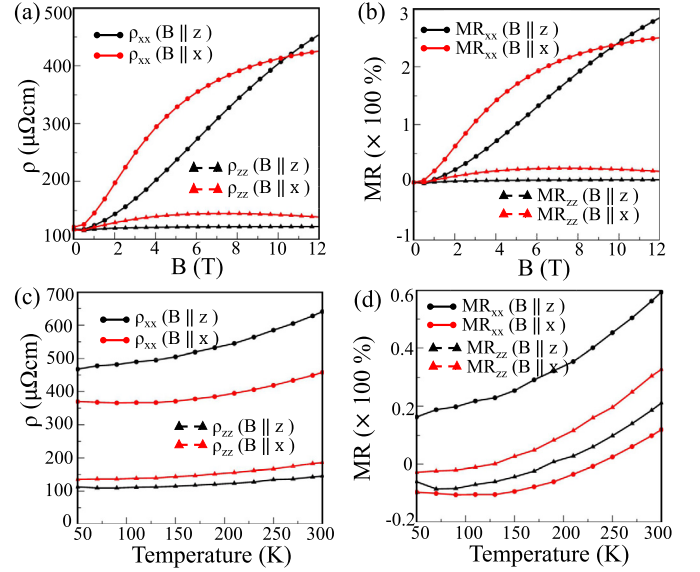


**Fig. 8.** (a) The resistivity and (b) the magnetoresistance as a function of magnetic field at a fixed temperature of 10 K, for  $E = E_F - 0.10$  eV. Temperature dependent resistivity, and magnetoresistance for a magnetic field value of 10 T are given in (c) and (d), respectively for  $E = E_F - 0.10$  eV.

the MR values [Fig. 7(d)]. Temperature-dependent MR values are much better than the ambient ones with  $MR_{zz}$  values of 65% and 80%, respectively when the magnetic field is subjected to 'z' and 'x' directions.

The magnetotransport properties at  $E = E_F - 0.10$  eV are given in Fig. 8. It is vivid from the plots that the transverse resistivity and MR values are non-saturating when the magnetic field is along 'z' direction. The MR values approach 280% at 12 T for 10 K. Temperature-dependent  $\rho_{zz}$  and  $MR_{zz}$  are also showing better results than the ambient ones with non-saturating behavior independent of magnetic field orientation [Fig. 8(c, d)]. The larger Fermi surface at  $E = E_F - 0.10$  eV compared with the ambient one for the hole-type band could be the possible reason for these observed variations [Fig. 7(e & f)]. Hole doping ( $E = E_F - 0.10$  eV) would be favorable for transverse magnetotransport properties when the magnetic field is applied along the 'x' direction. On the other hand, electron doping ( $E = E_F + 0.10$  eV) would be suitable when the field is switched to 'z' direction. The calculated magnetotransport properties are quite appreciable, with improvement up to 200% considering both hole and electron doping, which may entice experimentalists to investigate further.

## 6. Conclusion

In summary, we have demonstrated the theoretical modeling of electronic structure properties and the magnetotransport properties in  $Li_2BaSi$ . Fermi surface topology suggests that this system may host large magnetoresistance under the external magnetic field. Boltzmann transport theory is used to compute transport properties within relaxation time approximation. Transverse resistivity favors a high value of magnetoresistance with values of 75% under the magnetic field of 10 T at 10 K. These values are appreciable and in accord with the values of well-known semimetals. We have also calculated magnetotransport properties at Fermi energies, ( $E = E_F - 0.10$  eV) & ( $E = E_F + 0.10$  eV) to observe hole and electron doping effects. We observe the enhancement in transverse MR values up to 200% with non-saturating behavior at 10 K, when the field is along 'x' and 'z' directions for hole-type and electron-type doping. Overall, the investigated system might be a

good choice for future MR applications and awaits experimental verification.

### CRediT authorship contribution statement

**Vineet Kumar Sharma:** Writing – original draft, Methodology, Conceptualization. **V. Kanchana:** Writing – review & editing, Writing – original draft, Validation, Supervision, Conceptualization.

### Declaration of competing interest

The authors declare that they have no known competing financial interests or personal relationships that could have appeared to influence the work reported in this paper.

### Data availability

Data will be made available on request.

### Acknowledgement

VKS and VK would like to express their gratitude to IIT Hyderabad and C-DAC for providing computing resources. VKS would like to express gratitude to MoE for the fellowship.

### References

- [1] M.N. Baibich, J.M. Broto, A. Fert, F.N. Van Dau, F. Petroff, P. Etienne, G. Creuzet, A. Friederich, J. Chazelas, Giant magnetoresistance of (001)Fe/(001)Cr magnetic superlattices, *Phys. Rev. Lett.* 61 (1988) 2472–2475, <https://doi.org/10.1103/PhysRevLett.61.2472>, <https://link.aps.org/doi/10.1103/PhysRevLett.61.2472>.
- [2] G. Binash, P. Grünberg, F. Saurenbach, W. Zinn, Enhanced magnetoresistance in layered magnetic structures with antiferromagnetic interlayer exchange, *Phys. Rev. B* 39 (1989) 4828–4830, <https://doi.org/10.1103/PhysRevB.39.4828>, <https://link.aps.org/doi/10.1103/PhysRevB.39.4828>.
- [3] A.P. Ramirez, R.J. Cava, J. Krajewski, Colossal magnetoresistance in Cr-based chalcogenide spinels, *Nature* 386 (6621) (1997) 156–159, <https://doi.org/10.1038/386156a0>.
- [4] Y. Tokura, *Colossal Magnetoresistive Oxides*, Gordon and Breach Science Publishers, Amsterdam, the Netherlands, 2000.
- [5] J. Lenz, A review of magnetic sensors, *Proc. IEEE* 78 (6) (1990) 973–989, <https://doi.org/10.1109/5.56910>.
- [6] Y. Moritomo, A. Asamitsu, H. Kuwahara, Y. Tokura, Giant magnetoresistance of manganese oxides with a layered perovskite structure, *Nature* 380 (6570) (1996) 141–144, <https://doi.org/10.1038/380141a0>.
- [7] J. Daughton, GMR applications, *J. Magn. Magn. Mater.* 192 (2) (1999) 334–342, [https://doi.org/10.1016/S0304-8853\(98\)00376-X](https://doi.org/10.1016/S0304-8853(98)00376-X), <https://www.sciencedirect.com/science/article/pii/S030488539800376X>.
- [8] A.P. Ramirez, Colossal magnetoresistance, *J. Phys. Condens. Matter* 9 (39) (1997) 8171–8199, <https://doi.org/10.1088/0953-8984/9/39/005>.
- [9] K. Wang, D. Graf, L. Li, L. Wang, C. Petrovic, Anisotropic giant magnetoresistance in nbsb2, *Sci. Rep.* 4 (1) (2014) 7328, <https://doi.org/10.1038/srep07328>.
- [10] A.L. Friedman, J.L. Tedesco, P.M. Campbell, J.C. Culbertson, E. Aifer, F.K. Perkins, R.L. Myers-Ward, J.K. Hite, C.R. Eddy, G.G. Jernigan, D.K. Gaskill, Quantum linear magnetoresistance in multilayer epitaxial graphene, *Nano Lett.* 10 (10) (2010) 3962–3965, <https://doi.org/10.1021/nl101797d>.
- [11] K. Gopinadhan, Y.J. Shin, R. Jalil, T. Venkatesan, A.K. Geim, A.H.C. Neto, H. Yang, Extremely large magnetoresistance in few-layer graphene/boron–nitride heterostructures, *Nat. Commun.* 6 (1) (2015) 8337, <https://doi.org/10.1038/ncomms9337>.
- [12] T. Liang, Q. Gibson, M.N. Ali, M. Liu, R.J. Cava, N.P. Ong, Ultrahigh mobility and giant magnetoresistance in the Dirac semimetal cd3as2, *Nat. Mater.* 14 (3) (2015) 280–284, <https://doi.org/10.1038/nmat4143>.
- [13] Y. Zhao, H. Liu, C. Zhang, H. Wang, J. Wang, Z. Lin, Y. Xing, H. Lu, J. Liu, Y. Wang, S.M. Brombosz, Z. Xiao, S. Jia, X.C. Xie, J. Wang, Anisotropic Fermi surface and quantum limit transport in high mobility three-dimensional Dirac semimetal cd3as2, *Phys. Rev. X* 5 (2015) 031037, <https://doi.org/10.1103/PhysRevX.5.031037>, <https://link.aps.org/doi/10.1103/PhysRevX.5.031037>.
- [14] J. Feng, Y. Pang, D. Wu, Z. Wang, H. Weng, J. Li, X. Dai, Z. Fang, Y. Shi, L. Lu, Large linear magnetoresistance in Dirac semimetal cd3as2 with Fermi surfaces close to the Dirac points, *Phys. Rev. B* 92 (2015) 081306, <https://doi.org/10.1103/PhysRevB.92.081306>, <https://link.aps.org/doi/10.1103/PhysRevB.92.081306>.
- [15] X. Huang, L. Zhao, Y. Long, P. Wang, D. Chen, Z. Yang, H. Liang, M. Xue, H. Weng, Z. Fang, X. Dai, G. Chen, Observation of the chiral-anomaly-induced negative magnetoresistance in 3d Weyl semimetal taas, *Phys. Rev. X* 5 (2015) 031023, <https://doi.org/10.1103/PhysRevX.5.031023>, <https://link.aps.org/doi/10.1103/PhysRevX.5.031023>.
- [16] A.A. Soluyanov, D. Gresch, Z. Wang, Q. Wu, M. Troyer, X. Dai, B.A. Bernevig, Type-II Weyl semimetals, *Nature* 527 (7579) (2015) 495–498.
- [17] M.N. Ali, J. Xiong, S. Flynn, J. Tao, Q.D. Gibson, L.M. Schoop, T. Liang, N. Haldolaarachchige, M. Hirschberger, N.P. Ong, R.J. Cava, Large, non-saturating magnetoresistance in wte2, *Nature* 514 (7521) (2014) 205–208, <https://doi.org/10.1038/nature13763>.
- [18] F.C. Chen, H.Y. Lv, X. Luo, W.J. Lu, Q.L. Pei, G.T. Lin, Y.Y. Han, X.B. Zhu, W.H. Song, Y.P. Sun, Extremely large magnetoresistance in the type-II Weyl semimetal Mote2, *Phys. Rev. B* 94 (2016) 235154, <https://doi.org/10.1103/PhysRevB.94.235154>, <https://link.aps.org/doi/10.1103/PhysRevB.94.235154>.
- [19] Y.-Y. Lv, X. Li, B. Pang, L. Cao, D. Lin, B.-B. Zhang, S.-H. Yao, Y.B. Chen, J. Zhou, S.-T. Dong, S.-T. Zhang, M.-H. Lu, Y.-F. Chen, The relationship between anisotropic magnetoresistance and topology of Fermi surface in td-mote2 crystal, *J. Appl. Phys.* 122 (4) (2017) 045102, <https://doi.org/10.1063/1.4995951>.
- [20] N. Kumar, Y. Sun, N. Xu, K. Manna, M. Yao, V. Süss, I. Leermakers, O. Young, T. Förster, M. Schmidt, H. Borrmann, B. Yan, U. Zeitler, M. Shi, C. Felser, C. Shekhar, Extremely high magnetoresistance and conductivity in the type-II Weyl semimetals wp2 and mop2, *Nat. Commun.* 8 (1) (Nov 2017), <https://doi.org/10.1038/s41467-017-01758-z>.
- [21] A. Wang, D. Graf, Y. Liu, Q. Du, J. Zheng, H. Lei, C. Petrovic, Large magnetoresistance in the type-II Weyl semimetal wp2, *Phys. Rev. B* 96 (2017) 121107, <https://doi.org/10.1103/PhysRevB.96.121107>, <https://link.aps.org/doi/10.1103/PhysRevB.96.121107>.
- [22] R. Schönemann, N. Aryal, Q. Zhou, Y.-C. Chiu, K.-W. Chen, T.J. Martin, G.T. McCandless, J.Y. Chan, E. Manousakis, L. Balicas, Fermi surface of the Weyl type-II metallic candidate wp2, *Phys. Rev. B* 96 (2017) 121108, <https://doi.org/10.1103/PhysRevB.96.121108>, <https://link.aps.org/doi/10.1103/PhysRevB.96.121108>.
- [23] A. Pippard, *Magnetoresistance in Metals*, Cambridge Studies in Low Temperature Physics, Cambridge University Press, 1989, <https://books.google.co.in/books?id=D5XHMARD2ocC>.
- [24] H. Takatsu, J.J. Ishikawa, S. Yonezawa, H. Yoshino, T. Shishidou, T. Oguchi, K. Murata, Y. Maeno, Extremely large magnetoresistance in the nonmagnetic metal ydcoo2, *Phys. Rev. Lett.* 111 (2013) 056601, <https://doi.org/10.1103/PhysRevLett.111.056601>, <https://link.aps.org/doi/10.1103/PhysRevLett.111.056601>.
- [25] E. Mun, H. Ko, G.J. Miller, G.D. Samolyuk, S.L. Bud'ko, P.C. Canfield, Magnetic field effects on transport properties of ptsn4, *Phys. Rev. B* 85 (2012) 035135, <https://doi.org/10.1103/PhysRevB.85.035135>, <https://link.aps.org/doi/10.1103/PhysRevB.85.035135>.
- [26] K. Wang, D. Graf, L. Li, L. Wang, C. Petrovic, Anisotropic giant magnetoresistance in nbsb2, *Sci. Rep.* 4 (1) (2014) 7328, <https://doi.org/10.1038/srep07328>.
- [27] F. Fallah Tafti, Q. Gibson, S. Kushwaha, J.W. Krizan, N. Haldolaarachchige, R.J. Cava, Temperature-field phase diagram of extreme magnetoresistance, *Proc. Natl. Acad. Sci. USA* 113 (25) (2016) E3475–81.
- [28] J. He, C. Zhang, N.J. Ghimire, T. Liang, C. Jia, J. Jiang, S. Tang, S. Chen, Y. He, S.-K. Mo, C.C. Hwang, M. Hashimoto, D.H. Lu, B. Moritz, T.P. Devereaux, Y.L. Chen, J.F. Mitchell, Z.-X. Shen, Distinct electronic structure for the extreme magnetoresistance in ysb, *Phys. Rev. Lett.* 117 (2016) 267201, <https://doi.org/10.1103/PhysRevLett.117.267201>, <https://link.aps.org/doi/10.1103/PhysRevLett.117.267201>.
- [29] J. Xu, N.J. Ghimire, J.S. Jiang, Z.L. Xiao, A.S. Botana, Y.L. Wang, Y. Hao, J.E. Pearson, W.K. Kwok, Origin of the extremely large magnetoresistance in the semimetal ysb, *Phys. Rev. B* 96 (2017) 075159, <https://doi.org/10.1103/PhysRevB.96.075159>, <https://link.aps.org/doi/10.1103/PhysRevB.96.075159>.
- [30] R. Lou, Y.F. Xu, L.-X. Zhao, Z.-Q. Han, P.-J. Guo, M. Li, J.-C. Wang, B.-B. Fu, Z.-H. Liu, Y.-B. Huang, P. Richard, T. Qian, K. Liu, G.-F. Chen, H.M. Weng, H. Ding, S.-C. Wang, Observation of open-orbit Fermi surface topology in the extremely large magnetoresistance semimetal moas2, *Phys. Rev. B* 96 (2017) 241106, <https://doi.org/10.1103/PhysRevB.96.241106>, <https://link.aps.org/doi/10.1103/PhysRevB.96.241106>.
- [31] Z. Yuan, H. Lu, Y. Liu, J. Wang, S. Jia, Large magnetoresistance in compensated semimetals taas2 and nbas2, *Phys. Rev. B* 93 (2016) 184405, <https://doi.org/10.1103/PhysRevB.93.184405>, <https://link.aps.org/doi/10.1103/PhysRevB.93.184405>.
- [32] B. Shen, X. Deng, G. Kotliar, N. Ni, Fermi surface topology and negative longitudinal magnetoresistance observed in the semimetal nbas2, *Phys. Rev. B* 93 (2016) 195119, <https://doi.org/10.1103/PhysRevB.93.195119>, <https://link.aps.org/doi/10.1103/PhysRevB.93.195119>.
- [33] Y.-Y. Wang, H. Zhang, X.-Q. Lu, L.-L. Sun, S. Xu, Z.-Y. Lu, K. Liu, S. Zhou, T.-L. Xia, Extremely large magnetoresistance and electronic structure of tmsb, *Phys. Rev. B* 97 (2018) 085137, <https://doi.org/10.1103/PhysRevB.97.085137>, <https://link.aps.org/doi/10.1103/PhysRevB.97.085137>.
- [34] J. Du, Z. Lou, S. Zhang, Y. Zhou, B. Xu, Q. Chen, Y. Tang, S. Chen, H. Chen, Q. Zhu, H. Wang, J. Yang, Q. Wu, O.V. Yazyev, M. Fang, Extremely large magnetoresistance in the topologically trivial semimetal  $\alpha - wp_2$ , *Phys. Rev. B*

- 97 (2018) 245101, <https://doi.org/10.1103/PhysRevB.97.245101>, <https://link.aps.org/doi/10.1103/PhysRevB.97.245101>.
- [35] Y.-Y. Lv, X. Li, B. Pang, L. Cao, D. Lin, B.-B. Zhang, S.-H. Yao, Y.B. Chen, J. Zhou, S.-T. Dong, S.-T. Zhang, M.-H. Lu, Y.-F. Chen, The relationship between anisotropic magnetoresistance and topology of Fermi surface in *td-mote2* crystal, *J. Appl. Phys.* 122 (4) (2017) 045102, <https://doi.org/10.1063/1.4995951>.
- [36] B. Abeles, S. Meiboom, Galvanomagnetic effects in bismuth, *Phys. Rev.* 101 (1956) 544–550, <https://doi.org/10.1103/PhysRev.101.544>, <https://link.aps.org/doi/10.1103/PhysRev.101.544>.
- [37] J.E. Aubrey, Magnetoconductivity tensor for semimetals, *J. Phys. F, Met. Phys.* 1 (4) (1971) 493–497, <https://doi.org/10.1088/0305-4608/1/4/321>.
- [38] A. Laha, S. Malick, R. Singha, P. Mandal, P. Rambabu, V. Kanchana, Z. Hossain, Magnetotransport properties of the correlated topological nodal-line semimetal *ybcdge*, *Phys. Rev. B* 99 (2019) 241102, <https://doi.org/10.1103/PhysRevB.99.241102>, <https://link.aps.org/doi/10.1103/PhysRevB.99.241102>.
- [39] A. Laha, S. Mardanya, B. Singh, H. Lin, A. Bansil, A. Agarwal, Z. Hossain, Magnetotransport properties of the topological nodal-line semimetal *cacdsn*, *Phys. Rev. B* 102 (2020) 035164, <https://doi.org/10.1103/PhysRevB.102.035164>, <https://link.aps.org/doi/10.1103/PhysRevB.102.035164>.
- [40] V.K. Sharma, B. Singh, A.B. Sarkar, M.K. Gupta, R. Mittal, A. Agarwal, B. Singh, V. Kanchana, Topological phonons and electronic structure of *li2basi* class of semimetals, *J. Phys. Condens. Matter* 34 (12) (2022) 125502, <https://doi.org/10.1088/1361-648x/ac4441>.
- [41] X. Zhang, L. Jin, X. Dai, G. Chen, G. Liu, Ideal inner nodal chain semimetals in *Li(2) XY* ( $x = \text{ca, ba}$ ;  $Y = \text{si, ge}$ ) materials, *J. Phys. Chem. Lett.* 9 (18) (2018) 5358–5363.
- [42] G. Kresse, J. Furthmüller, Efficiency of ab-initio total energy calculations for metals and semiconductors using a plane-wave basis set, *Comput. Mater. Sci.* 6 (1) (1996) 15–50, [https://doi.org/10.1016/0927-0256\(96\)00008-0](https://doi.org/10.1016/0927-0256(96)00008-0), <https://www.sciencedirect.com/science/article/pii/S0927025696000080>.
- [43] G. Kresse, J. Furthmüller, Efficient iterative schemes for ab initio total-energy calculations using a plane-wave basis set, *Phys. Rev. B* 54 (1996) 11169–11186, <https://doi.org/10.1103/PhysRevB.54.11169>, <https://link.aps.org/doi/10.1103/PhysRevB.54.11169>.
- [44] J.P. Perdew, K. Burke, M. Ernzerhof, Generalized gradient approximation made simple, *Phys. Rev. Lett.* 77 (1996) 3865–3868, <https://doi.org/10.1103/PhysRevLett.77.3865>, <https://link.aps.org/doi/10.1103/PhysRevLett.77.3865>.
- [45] J.-L. Calais, Density-functional theory of atoms and molecules. R.G. Parr and W. Yang, Oxford University Press, New York, Oxford, 1989. IX + 333 pp. Price £45.00, *Int. J. Quant. Chem.* 47 (1) (1993) 101, <https://doi.org/10.1002/qua.560470107>.
- [46] D. Stoiber, M. Bobnar, P. Höhn, R. Niewa, Lithium alkaline earth tetrelides of the type *li2aett* ( $a = \text{ca, ba}$ ,  $t = \text{si, ge, sn, pb}$ ): synthesis, crystal structures and physical properties, *Z. Naturforsch., B* 72 (11) (2017) 847–853.
- [47] H.J. Monkhorst, J.D. Pack, Special points for Brillouin-zone integrations, *Phys. Rev. B* 13 (1976) 5188–5192, <https://doi.org/10.1103/PhysRevB.13.5188>, <https://link.aps.org/doi/10.1103/PhysRevB.13.5188>.
- [48] P.E. Blöchl, O. Jepsen, O.K. Andersen, Improved tetrahedron method for Brillouin-zone integrations, *Phys. Rev. B* 49 (1994) 16223–16233, <https://doi.org/10.1103/PhysRevB.49.16223>, <https://link.aps.org/doi/10.1103/PhysRevB.49.16223>.
- [49] G.K. Madsen, D.J. Singh, Boltztrap. A code for calculating band-structure dependent quantities, *Comput. Phys. Commun.* 175 (1) (2006) 67–71, <https://doi.org/10.1016/j.cpc.2006.03.007>, <https://www.sciencedirect.com/science/article/pii/S0010465506001305>.
- [50] T.J. Scheidmantel, C. Ambrosch-Draxl, T. Thonhauser, J.V. Badding, J.O. Sofo, Transport coefficients from first-principles calculations, *Phys. Rev. B* 68 (2003) 125210, <https://doi.org/10.1103/PhysRevB.68.125210>, <https://link.aps.org/doi/10.1103/PhysRevB.68.125210>.
- [51] L. Jodin, J. Tobola, P. Pecheur, H. Scherrer, S. Kaprzyk, Effect of substitutions and defects in half-Heusler FeVsb studied by electron transport measurements and kkr-cpa electronic structure calculations, *Phys. Rev. B* 70 (2004) 184207, <https://doi.org/10.1103/PhysRevB.70.184207>, <https://link.aps.org/doi/10.1103/PhysRevB.70.184207>.
- [52] L. Chaput, P. Pêcheur, J. Tobola, H. Scherrer, Transport in doped skutterudites: ab initio electronic structure calculations, *Phys. Rev. B* 72 (2005) 085126, <https://doi.org/10.1103/PhysRevB.72.085126>, <https://link.aps.org/doi/10.1103/PhysRevB.72.085126>.
- [53] N. Marzari, D. Vanderbilt, Maximally localized generalized Wannier functions for composite energy bands, *Phys. Rev. B* 56 (1997) 12847–12865, <https://doi.org/10.1103/PhysRevB.56.12847>, <https://link.aps.org/doi/10.1103/PhysRevB.56.12847>.
- [54] A.A. Mostofi, J.R. Yates, G. Pizzi, Y.-S. Lee, I. Souza, D. Vanderbilt, N. Marzari, An updated version of Wannier90: a tool for obtaining maximally-localised Wannier functions, *Comput. Phys. Commun.* 185 (8) (2014) 2309–2310, <https://doi.org/10.1016/j.cpc.2014.05.003>, <http://www.sciencedirect.com/science/article/pii/S001046551400157X>.
- [55] Q. Wu, S. Zhang, H.-F. Song, M. Troyer, A.A. Soluyanov, WannierTools: an open-source software package for novel topological materials, *Comput. Phys. Commun.* 224 (2018) 405–416, <https://doi.org/10.1016/j.cpc.2017.09.033>, arXiv:1703.07789.
- [56] M.P.L. Sancho, J.M.L. Sancho, J.M.L. Sancho, J. Rubio, Highly convergent schemes for the calculation of bulk and surface Green functions, *J. Phys. F, Met. Phys.* 15 (4) (1985) 851–858, <https://doi.org/10.1088/0305-4608/15/4/009>.
- [57] S.B. Dugdale, Life on the edge: a beginner's guide to the Fermi surface, *Phys. Scr.* 91 (5) (2016) 053009, <https://doi.org/10.1088/0031-8949/91/5/053009>.
- [58] S. Zhang, Q. Wu, Y. Liu, O.V. Yazyev, Magnetoresistance from Fermi surface topology, *Phys. Rev. B* 99 (2019) 035142, <https://doi.org/10.1103/PhysRevB.99.035142>.
- [59] S. Li, Z. Guo, D. Fu, X.-C. Pan, J. Wang, K. Ran, S. Bao, Z. Ma, Z. Cai, R. Wang, R. Yu, J. Sun, F. Song, J. Wen, Evidence for a Dirac nodal-line semimetal in *sras3*, *Sci. Bull.* 63 (9) (2018) 535–541, <https://doi.org/10.1016/j.scib.2018.04.011>, <https://www.sciencedirect.com/science/article/pii/S2095927318301683>.
- [60] S. Malick, J. Singh, A. Laha, V. Kanchana, Z. Hossain, D. Kaczorowski, Electronic structure and physical properties of *euaus* single crystal, *Phys. Rev. B* 105 (2022) 045103, <https://doi.org/10.1103/PhysRevB.105.045103>, <https://link.aps.org/doi/10.1103/PhysRevB.105.045103>.